

Differential losses in Bragg fibers

C. Martijn de Sterke, I. M. Bassett, and Arthur G. Street

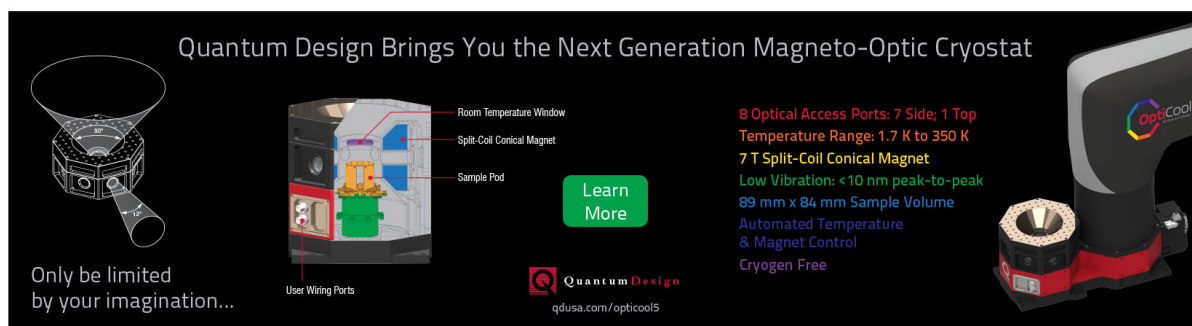
Citation: *Journal of Applied Physics* **76**, 680 (1994); doi: 10.1063/1.357811

View online: <https://doi.org/10.1063/1.357811>

View Table of Contents: <http://aip.scitation.org/toc/jap/76/2>

Published by the *American Institute of Physics*

Quantum Design Brings You the Next Generation Magneto-Optic Cryostat



Only be limited by your imagination...

Learn More

Quantum Design
qdusa.com/opticool5

8 Optical Access Ports: 7 Side; 1 Top
Temperature Range: 1.7 K to 350 K
7 T Split-Coil Conical Magnet
Low Vibration: <10 nm peak-to-peak
89 mm x 84 mm Sample Volume
Automated Temperature & Magnet Control
Cryogen Free

Differential losses in Bragg fibers

C. Martijn de Sterke and I. M. Bassett

School of Physics, and Optical Fibre Technology Centre, University of Sydney, NSW 2006, Australia

Arthur G. Street^{a)}

School of Physics, University of Sydney, NSW 2006, Australia

(Received 29 November 1993; accepted for publication 29 March 1994)

Most dielectric waveguides depend for guidance on total internal reflection within a region of elevated refractive index. A little-explored alternative to this is Bragg reflection. Here we consider a "Bragg" optical fiber in which a cylindrical Bragg grating is used to inhibit radial power flow. We find that such Bragg fibers can be guaranteed to be effectively single-moded, with no polarization degeneracy; the electric field in this fundamental mode is purely azimuthal (transverse electric polarized).

I. INTRODUCTION

Though the guiding of light in standard optical fibers is achieved by total internal reflection, this is not the only mechanism which can be used to confine radiation. An alternative is Bragg reflection, which takes place in structures such as shown in Fig. 1. It occurs when the light which is Fresnel reflected off the interfaces shown in Fig. 1 interferes constructively; it is thus strongest when all these reflected wavelets are in phase. Although the field is represented by a traveling wave in each layer, the overall transverse profile of the field intensity is exponentially decaying in the outward direction, thus indicating that radiation is confined. Following Yeh *et al.*¹ and Doran *et al.*² we refer to fibers which confine light in this way as Bragg fibers.

Because the field intensity in Bragg fibers decays exponentially, confinement can be improved by adding layers. A properly bound mode would thus require an *infinite* number. This implies that in any practical system with a *finite* number of layers all modes are, to some degree, leaky.³ Indeed, it has been pointed out by Doran *et al.*² that Bragg fibers support an infinite number of modes, all of which are lossy. But if in some frequency interval the loss of one of these modes is significantly less than that of all others, then the fiber is *de facto* single moded. This differs from standard fibers where confinement is assured by total internal reflection at the single interface between core and cladding. Standard fibers thus have properly bound modes if the cladding can be assumed to extend to infinity, a situation which is easily approximated in practice.

Previous studies of Bragg fibers were motivated by possible applications in long-distance communications. Yeh *et al.*¹ have suggested that if one of the fiber modes has significantly less loss than all other modes, Bragg fibers can act as modal filters. Doran *et al.*² on the other hand, have shown that Bragg fibers do not offer realistic possibilities for low-loss propagation. They base this conclusion on two arguments. The first of these is practical: tight tolerances make the fabrication of Bragg fibers very difficult. The second is more fundamental: even if the structure were fabricated per-

fectly, the launching of the modes would be very inefficient. For the particular example of a fiber with a loss of about 10 dB/km, Doran *et al.*² estimate that only 1 part in 10^6 of the incoming energy could be launched into the desired mode from a conventional single transverse mode source.

Our motivation for studying Bragg fibers is not long-distance telecommunications, and we therefore do not seek ultra-low fiber losses. Rather, our interest is driven by possibilities for obtaining unusual modal profiles and, like Yeh *et al.*,¹ for obtaining modal filters. Such effects do not require long propagation distances, and moderate losses can thus be tolerated. We thus focus on differential losses between the modes to estimate the modal discrimination. The lower emphasis on absolute losses has important implications for the arguments used by Doran *et al.*² to show that Bragg fibers are impractical for low-loss applications: fabrication tolerances of Bragg fibers in which higher losses are tolerated are less severe, while, adopting their method to describe coupling processes, the coupling efficiency into a mode in such a fiber can be larger. In addition, a recently developed class of surface emitting semiconductor lasers have modal patterns with an intensity null at the center, which appear to match the required field profile quite well.⁴ We return to this point below.

Since the modal profiles and modal losses are only weakly dependent on the refractive indices, we neglect henceforth the dispersion of the constituent materials. This has the important advantage that the properties of structures can easily be scaled if the wavelength of the radiation is scaled in the same way. Of course this scaling is not allowed if the refractive indices of the constituents are wavelength dependent.

II. GENERAL CONSIDERATIONS

The structures we consider have a piecewise continuous refractive index distribution $n(r)$ (Fig. 1), taking on the values n_1 and n_2 with, say, $n_1 < n_2$. Now as mentioned, if the Bragg condition is satisfied then wavelets reflected off all interfaces interfere constructively. Since for Bragg fibers this effect occurs in the direction perpendicular to that of propagation, this condition involves the transverse wavenumber κ , where

^{a)}Present address: Department of Mathematics, University of New South Wales, Kensington, NSW 2033, Australia.

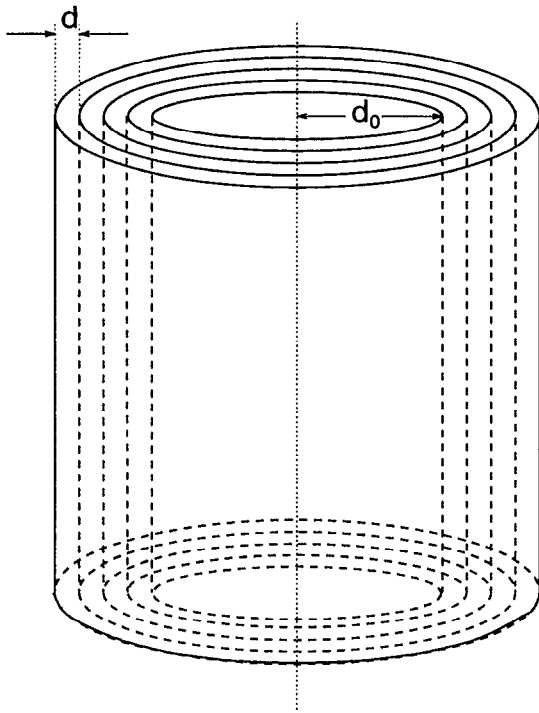


FIG. 1. Schematic of the Bragg fibers we are considering here. The refractive index distribution is taken to be uniform in the longitudinal direction, and consists of concentric rings in the transverse direction. Here we take all rings to have the same thickness d , while the radius of the inner part is d_0 . The refractive indices of the layers is alternately n_1 and n_2 .

$$\kappa = \sqrt{\frac{n^2 \omega^2}{c^2} - \beta^2} = \frac{\omega}{c} \sqrt{n^2 - N^2}, \quad (1)$$

where ω the (angular) frequency of the field, c is the speed of light, β is the propagation constant, which is taken to be real here, and in the last equality we have used the mode index $N \equiv \beta c / \omega$. To ensure that the confinement effects we observe are due purely to Bragg reflection, we take $N < n_1$, so that no total internal reflection occurs. This is in contrast to standard fibers where N must be taken *between* the refractive indices of core and cladding. Further, again in contrast to standard fibers, we give the center of the structure the lowest refractive index, so that there $n = n_1$.

Since the achievable refractive index modulation in a fiber is small,⁶ n can be considered to be approximately constant. Also, as $r \rightarrow \infty$, where the curvature of the layers can be neglected, $n(r)$ must be periodic for Bragg reflection to occur.⁵ With these simplifications it is easy to see that Bragg reflection occurs when all layers have the same thickness d , and when the phase in the transverse direction changes by $\pi/2$ in each layer, or

$$\bar{\kappa} = M \frac{\pi}{2d}, \quad (2)$$

where $\bar{\kappa}$ is the transverse wavenumber [Eq. (1)] associated with the average refractive index $\bar{n} \equiv (n_1 + n_2)/2$, and the positive integer M indicates the Bragg reflection order. Here we only consider first order Bragg reflection where $M = 1$. Note that the approximation leading to Eq. (2) fails when

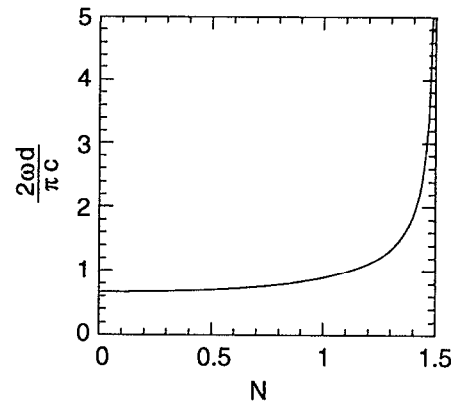


FIG. 2. Dimensionless frequency $2\omega d / (\pi c)$ for which Bragg reflection occurs as a function of the mode index N for a Bragg fiber with $\bar{n} = 1.5$ and with small refractive index modulation in the asymptotic limit in which the curvature of the rings is negligible.

$N \rightarrow n_1$. Although Eq. (2) can easily be generalized we do not do so here in view of the rigorous treatment discussed in Sec. III.

Figure 2 shows, using Eqs. (1) and (2), where first order Bragg reflection occurs in the asymptotic limit for a structure with an average refractive index $\bar{n} = 1.5$, and with rings with a thickness d . Since we neglect material dispersion, the properties of structures with the same refractive indices but different ring thicknesses can be found by appropriately scaling the results; on the vertical axis we thus show the dimensionless frequency $2\omega d / (\pi c)$. Figure 2 shows that Bragg structures can lead to confinement of light with propagation constants such that $0 < \beta < n_1 \omega / c$. At the high end of this interval (to the right in Fig. 2) the light reflects grazingly off the interfaces, while at the lower end (on the left in Fig. 2) the light reflects almost perpendicularly. This latter limit is similar to the structures studied by Ergodan *et al.*⁴ in the context of concentric-circle-grating surface-emitting semiconductor lasers. Previous discussions of Bragg fibers, particularly Ref. 2 indicate that grazing reflection angles are advantageous as the Fresnel reflection is then strongest, thus improving confinement. However, since we are interested in differential losses, rather than in the losses themselves, this is less of an issue for our applications.

III. RIGOROUS TREATMENT

It is well-known that in each of the layers of a Bragg fiber the fields can be written as superpositions of inward and outward propagating waves, which must be suitably matched at the interfaces. While our procedure, which differs in implementation from that in Refs. 1 and 2 is outlined in the Appendix, we here briefly discuss the main points. Following treatments of standard optical fibers^{7,8} we write the modal electric and magnetic fields as the real part of

$$\mathbf{E}(\mathbf{r}, t) = \mathbf{e}(\mathbf{r}) e^{i(\beta z - \omega t)} e^{im\varphi}, \quad (3)$$

$$\mathbf{H}(\mathbf{r}, t) = \frac{1}{Z} \mathbf{h}(\mathbf{r}) e^{i(\beta z - \omega t)} e^{im\varphi}, \quad (4)$$

where m is the azimuthal parameter, and Z is the vacuum impedance. The inclusion of the latter assures that these modified magnetic field components \mathbf{h} have the same dimensions as the electric field components \mathbf{e} ; as a result some expressions are simplified, and are cast in a more convenient form for numerical analysis. It is well known that if the fiber is cylindrically symmetric, then all field components can be found in terms of the longitudinal components $e_z(r)$ and $h_z(r)$.^{7,8} Because of the cylindrical symmetry, in each layer these components can be written as superpositions of suitably chosen Bessel functions, subject to the appropriate boundary conditions at the interfaces. However, the boundary conditions not only involve e_z and h_z , but also two other field components, usually taken to be e_ϕ and h_ϕ . In other treatments^{1,2} all four field components are therefore followed through the fiber. Such a calculation can be cast in matrix form, and, although straightforward, requires 4×4 matrices. An alternative approach has been given by Chew,⁹ in which only e_z and h_z are tracked through the system; this method can also be cast in matrix form, making use of 2×2 matrices. The drawback is that finding these smaller matrices is not as straightforward as in the method described above: in the process the azimuthal field components must be generated in order to cross the interfaces.

As mentioned, in Chew's method⁹ one follows the longitudinal field components through the system. In the Appendix we demonstrate that in the absence of losses, in the innermost region these field components can be written as

$$\begin{bmatrix} e_z \\ h_z \end{bmatrix} = (H_m^+(\kappa_1 r) + H_m^-(\kappa_1 r) \tilde{R}_{m,12}) \mathbf{a}_1, \quad (5)$$

where H_m^+ and H_m^- are Hankel functions of order m , of the first and second kind, respectively, indicating outward and inward propagating fields. The vector \mathbf{a}_1 determines the relative amplitudes of the electric and magnetic field components propagating outwards, while the matrix $\tilde{R}_{m,12}$ gives the relation between the electric and magnetic field components of the inward and outward propagating fields, and is thus a *reflection matrix*; the subscript m indicates that this matrix depends on the azimuthal parameter. Note that $\tilde{R}_{m,12}$ includes all multiple reflections in the entire structure. Once this matrix is known we can find the modes of the structure as follows: as $r \rightarrow 0$ the Hankel functions diverge; the only linear combination which does not diverge is the sum $H^+ + H^-$. So in order to have finite fields at the center, the reflection matrix must have an eigenvalue of unity, or

$$\tilde{R}_{m,12} \mathbf{a}_1 = \mathbf{a}_1. \quad (6)$$

Recall that only Bragg fibers with an infinite number of layers have properly bound modes; for finite structures we would thus not expect the reflection matrix to have an eigenvalue of unity. But, since we tolerate some losses, our "modes" are characterized by eigenvalues "close" to unity. But we know that such eigenvalues lead to the field diverging at the center. This apparent problem arises since if the structure is lossless, then energy conservation requires that the transverse energy flow through the system be conserved. Because of the condition in Eq. (6) this means that we are limiting ourselves, just as Yeh *et al.*¹ and Doran *et al.*² to

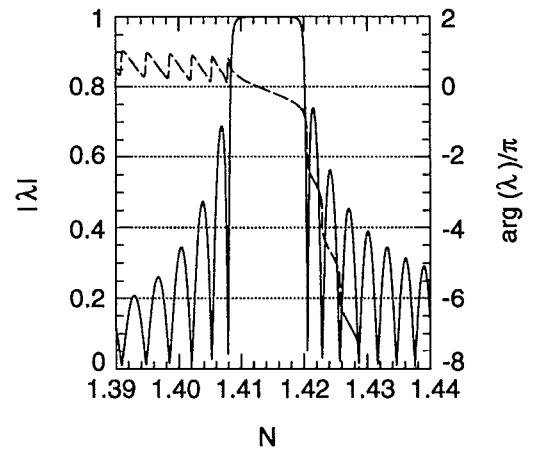


FIG. 3. Modulus (solid line; left-hand scale), and phase divided by π (dashed line; right-hand scale) of the lower right element of the matrix $\tilde{R}_{0,12}$ as a function of the mode index N , for a structure consisting of 100 layers, layer thicknesses of $1 \mu\text{m}$, inner radius $d_0 = 2.50 \mu\text{m}$, and refractive indices 1.49 and 1.51. Modes exist when this element equals unity; the figure thus shows a mode for $N = 1.4126$.

fields in which this energy flow vanishes. For a finite system with real propagation constant this would imply a source at infinity providing just enough energy so as to cancel the energy losses due to the imperfect confinement, or a source at the origin. In an alternative treatment the propagation constant β is given a small imaginary part, expressing energy loss. This would allow one to describe fields which, without sources, do not diverge at the center, and which do not have energy flowing in from infinity. But such a treatment is more complicated, and, if the losses are sufficiently small, then the slightly unrealistic situation considered here is a good approximation.

As noted in the Appendix, when $m = 0$ the reflection matrix $\tilde{R}_{0,12}$ is diagonal. This implies, just as in standard fibers, that the electric and magnetic fields do not mix; the modes can then be classified as either transverse electric (TE) with $h_z = 0$, or transverse magnetic (TM) with $e_z = 0$. For other values of m , $\tilde{R}_{m,12}$ is not diagonal, indicating that, again just as in standard fibers, the associated modes are hybrid, having both longitudinal magnetic and electric field components. However, because $+m$ and $-m$ lead to a reflection matrix with the same eigenvalues, these higher order modes are degenerate: each mode for $m > 0$ is paired with a counterpart with $m < 0$ and the same wavenumber.

The eigenvalues of the reflection matrix have a simple interpretation: they give the ratio of the amplitudes of the incoming and the outgoing cylindrical waves in the structure, and thus represent an (amplitude) reflection coefficient—indeed, consistent with the discussion above, one would only expect a bound mode when this reflection coefficient equals unity. To illustrate this interpretation, which is also discussed in the appendix, we consider Fig. 3, which shows for radiation with $\omega/c = 3.14 \times 10^6 \text{ m}^{-1}$, and a structure with 100 layers,⁶ layer thicknesses $d = 1 \mu\text{m}$, a radius of the innermost region of $d_0 = 2.50 \mu\text{m}$, and refractive indices $n_1 = 1.49$ and $n_2 = 1.51$, the modulus (solid lines; left-hand

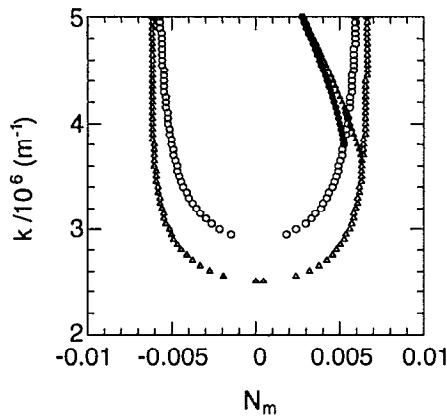


FIG. 4. Position of the $m=0$ modes in a structure with 100 layers, $n_1=1.49$, $n_2=1.51$, $d=1\text{ }\mu\text{m}$, and $d_0=3.25\text{ }\mu\text{m}$, as a function of $N_M=N-N_B$, the mode index with respect to the Bragg condition, and the vacuum wavenumber k . The TE (TM) modes are indicated by the closed triangles (circles). The open symbols indicate the regions for which the fiber provides sufficient confinement.

scale), and the argument divided by π (long dashed lines; right-hand scale) of the bottom right element of $\bar{R}_{0,12}$ as a function of frequency. Since for $m=0$ the matrix is diagonal this element corresponds to one of the eigenvalues of the reflection matrix, in fact that associated with the TE modes. The dotted horizontal lines indicate where the phase is an integer multiple of 2π .

Figure 3 shows the existence of a mode for $N=1.4126$, corresponding to a propagation constant $\beta=4.435\times 10^6\text{ m}^{-1}$. This is consistent with Eqs. (1) and (2), which indicate that for our parameters the Bragg condition is satisfied at $N=1.414$. Indeed, the figure shows that the modulus is (very nearly) equal to unity for a range of mode indices centered about this value, while elsewhere it is much smaller. Actually, for this structure the modulus of the eigenvalue is slightly less than unity and equals 0.99974, indicating imperfect confinement, and thus a small energy leakage. As expected, the actual position of the mode strongly depends on the radius of the innermost region d_0 . For example, for $d_0=2.60\text{ }\mu\text{m}$ and all other parameters unchanged, the mode shifts to $N=1.4139$.

We have seen that the eigenvalue λ represents the amplitude reflection coefficient for a mode—if $|\lambda|<1$ the structure does not act as a perfect mirror and cannot confine light. If $|\lambda|\approx 1$ then modes only exist if the phase angle of λ vanishes—clearly this corresponds to a phase condition, specifying that modes only exist if some cavity requirement is met.

IV. RESULTS

As a first example we show in Fig. 4 results for a structure with 100 rings with consecutive high and low refractive indices of $n_1=1.49$ and $n_2=1.51$, $d=1\text{ }\mu\text{m}$, $d_0=3.25\text{ }\mu\text{m}$, for $m=0$. Because the modes occur in the narrow region around the Bragg reflection curve of the structure (such as Fig. 2), we plot for convenience on the horizontal axis $N_M=N-N_B$, where N_B is the mode index for which Bragg

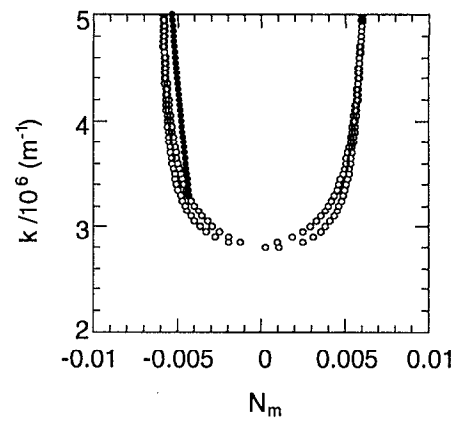


FIG. 5. Position of the $m=1$ modes in the same structure as in Fig. 4. The closed symbols again indicate the modes. Though for $m=1$ the modes come in pairs as well (as in Fig. 4), only one of these two experience enough confinement by the structure to be shown here. As in Fig. 4, the open symbols indicate the region for which the system provides sufficient confinement; since the distinction between the two modes is not as firm as for $m=0$, only circles are used.

reflection occurs [Eqs. (1) and (2)]. For $N_M=0$, the Bragg condition Eq. (2) is thus exactly satisfied. The closed symbols in Fig. 4 give the position of the modes as a function of the vacuum wavenumber $k=\omega/c$. A mode is taken to “exist” if $|\lambda|>0.999$, and $\arg(\lambda)=0$, the former condition specifying that the structure provides enough reflectivity, and the latter corresponding to the cavity condition discussed above. The open symbols indicate the region for which $|\lambda|>0.999$. The regions bounded by the open circles indicate, therefore, the region for which modes can exist—outside these regions the structure simply does not provide sufficient confinement. The open symbols in Fig. 4 define two curves. These are associated with the two eigenvalues of the reflection matrix; for $m=0$ these correspond to TE and TM polarized modes. Since the Fresnel reflection coefficient of TE polarized light is larger than that of TM (see e.g., Born and Wolf¹⁰), we know that the triangles refer to TE polarization, and the circles denote TM.

Figure 5 shows results for the same structure as in Fig. 4, except that $m=1$. Clearly the two figures have the same general structure. Though we would expect two $m=1$ modes only one of these has sufficient confinement, and only one is thus indicated. The region where the reflection coefficient exceeds 0.999 is indicated by the open symbols; now that the modes are hybrid we indicate all modes by circles. We have repeated these calculations for values $m>1$, and find that the results are very similar, though the positions of the modes of course differ. We therefore do not show these results here.

As discussed in Sec. I, we are concerned here with differential losses. To find the loss we apply an approximate procedure developed for planar waveguides,¹¹ to the cylindrical structures considered here. Such a calculation results in an expression for the power attenuation coefficient 2α , i.e., $I(z)\propto \exp(-2\alpha z)$, where I is the intensity, which reads

$$2\alpha = \frac{2}{R_{\text{eff}}} T \frac{\kappa}{\beta}, \quad (7)$$

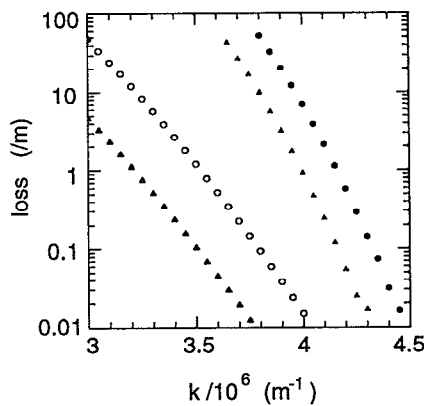


FIG. 6. Losses for the $m=0$ modes for the same structure as that in Fig. 4. The meaning of the symbols is the same as in Fig. 4 as well. The closed symbols indicate the actual losses of the modes, while the open symbols give the minimum achievable loss. Such minimum losses can, for a particular frequency, be achieved by adjusting d_0 . Clearly the minimum losses for TM modes are larger than those for TE modes. Note that a power attenuation coefficient $2\alpha \text{ m}^{-1}$ corresponds to a loss of $8.68\alpha \text{ dB/m}$.

where R_{eff} is an effective modal radius, and the transmissivity T is given by

$$T = 1 - |\lambda|^2. \quad (8)$$

While in conventional waveguides and fibers the modal size roughly equals that of the guiding layer, this approximation is here not valid since the reflector is distributed. We thus approximate the modal size to be the radius where the intensity drops to $1/e$ of its peak value. This radius can be found approximately by solving

$$e^{-R/R_{\text{eff}}} = T, \quad (9)$$

since the transmissivity T roughly equals the intensity ratio at the structure's outer radius \bar{R} , and the center. Using Eq. (9) into Eq. (7) we find that the loss is roughly given by

$$2\alpha = \frac{2}{\bar{R}} \ln \left[\frac{1}{T} \right] T \frac{\kappa}{\beta}.$$

Results of such a calculation, for $m=0$ for the structure as in Figs. 4 and 5 is shown in Fig. 6, with the symbols having the same meaning: the round (triangular) symbols refer to TM (TE) polarization; the closed symbols refer to the actual modes, the open symbols refer only to the strength of the reflectivity, and represent the lowest possible loss at a particular k . As we discuss below, the idea is then that by choosing the inner radius appropriately, the cavity condition can always be chosen such that this minimum loss can be reached. Figure 6 is consistent with Fig. 4 in that the losses of the TE modes are lower than those of the TM modes. We note that within our model, the losses are predicted to decrease monotonically with increasing k . This can of course not be sustained as Rayleigh scattering and fabrication imperfections in practice determine the minimum achievable loss.

Finally, in Fig. 7 we show the losses for the $m=1$ modes (Fig. 5); they are clearly much higher than those in Fig. 6.

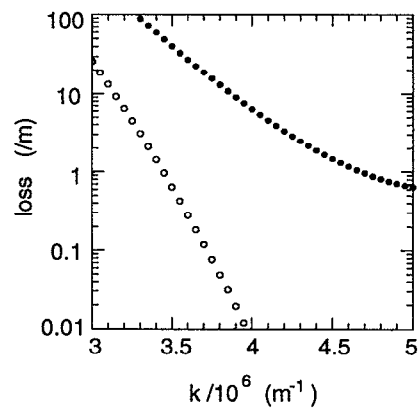


FIG. 7. Same as Fig. 6, but for the $m=1$ modes. Since the distinction between the modes is not as clear as for $m=0$, only circles are used.

This is not surprising since Fig. 5 shows that the $m=1$ modes exist only far from the Bragg condition. More interesting is a comparison of the minimum obtainable losses. Here we see that the minimum losses of the TE modes are always lower than those of the $m=1$ modes by over a factor of 5. Comparison with the losses of $m>1$ modes has shown that this is a general pattern. The minimum TE losses are always smaller than the minimum TM losses, while the losses of all other modes are very similar, and are between those for TE and TM. The ratio of the losses of the various modes is remarkably independent of frequency, while the actual loss level varies over several orders of magnitude. We have found this to be true for all cases we have studied. In Sec. V we discuss this property and argue that it is general. It has important consequences: it implies that the losses of the TE mode can always be made smaller than those of any other mode, irrespective of the cavity conditions of any of the higher modes. A Bragg fiber is then thus *de facto* a truly (i.e., nondegenerate) single mode fiber. This single mode is TE polarized. To illustrate this behavior we refer to Fig. 8, which shows the modes for the same structure as that discussed above, but with $d_0 = 2.7 \mu\text{m}$. The meaning of the symbols is unchanged. The figure clearly shows that both the TE and the TM modes almost attain the minimum loss which each can reach in this structure at these frequencies. We have achieved this by choosing d_0 such that the mode frequency is at the Bragg frequency so that $N_M = 0$. The TM mode is seen to be more than ten times as lossy as the TE mode. The open squares indicate the minimum achievable losses of the $m=1$ and $m=2$ modes. We note that the minimum losses of higher order modes are comparable. Clearly the losses of the higher order modes are at least a factor 6 higher than those of TE irrespective of the cavity condition, showing that the TE mode is the *de facto* fundamental mode at this frequency.

Finally, in Fig. 9 we show two of the field components of the TE mode at $k = 3.3 \times 10^6 \text{ /m}$: the h_z component (solid line) and the e_ϕ component (dashed line). The squares indicate the positions of the interfaces. Further, both components oscillate with a period of four layers (two periods) of the structure. As expected, although the fields are running waves in each of the layers, both field components are seen to have

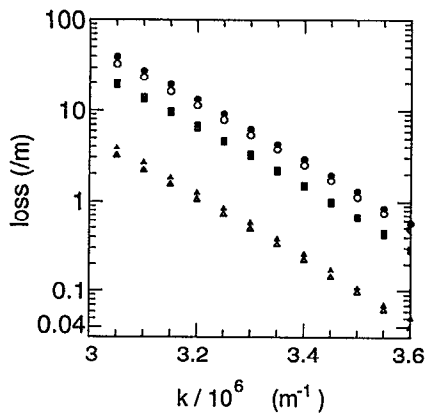


FIG. 8. Losses and minimum losses for various modes in a structure with 100 layers, a layer thickness of $1 \mu\text{m}$, and $d_0 = 2.7 \mu\text{m}$. The triangles refer to the TE mode, while the circles refer to TM. The closed symbols denote the actual modal losses, while the open symbols refer to the minimum achievable losses based on the strength of the mirrors. The open squares denote the minimum losses of the $m=1$ and $m=2$ modes; the minimum losses of yet higher order modes are comparable.

an overall envelope which decays exponentially in the transverse direction. Note, finally, that just like the TE modes of standard fibers, the electric field strength in the center vanishes.

V. DISCUSSION AND CONCLUSIONS

In Sec. IV we showed that the loss of one of the TE modes can be made smaller than the loss of all other modes. It is clear why TM modes have larger losses; it follows from the Fresnel reflection coefficients of plane waves.¹⁰ Indeed we have found that TM modes are not confined at all at Brewster's angle, where the reflection coefficient for TM waves vanishes. A heuristic argument explaining why the losses of all other modes exceed that of this TE mode, is that, locally, the relative orientation of the field and the interfaces

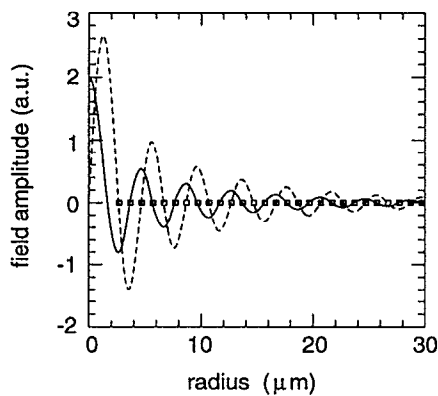


FIG. 9. Amplitudes of the h_z (solid line) and e_ϕ (dashed line) components of the TE mode in Fig. 8 at $k = 3.3 \times 10^6/\text{m}$. The squares indicate the layer interfaces. Since the mode index $N = 1.423462$ is significantly smaller than the lowest refractive index of the structure ($n_1 = 1.49$) the mode does not propagate nearly parallel to the axis, and the h_z component, which usually is a minor field component, is of the same order of magnitude as e_ϕ .

varies continuously between parallel (as in TE modes), and perpendicular (as in TM modes). The losses of the hybrid modes would then be expected to be between those of TE- and TM-polarized modes as well. The differential loss between TE and TM modes in the example we considered was well over ten. This ratio decreases when the number of layers is reduced. For example, for a cylindrical structure with 50 layers the ratio is roughly four.

Another important difference between the modes of Bragg fibers and those of standard fibers is that the field of the latter decays exponentially, while the field *outside* a Bragg fiber decays very slowly ($\propto 1/\sqrt{r}$). Bragg fibers are therefore much more sensitive to the external medium than standard fibers, which may be a desirable property for external modulation of the propagation characteristics, or in applications such as fiber sensors.

Since the losses of the systems we consider are higher than those of Yeh *et al.*,¹ and Doran *et al.*,² Doran's method to estimate launching efficiencies would imply that the launching requirements of lossy modes are not quite as severe. Still, since the modal profile differs strongly from those of standard fiber modes and standard diode laser sources the mode overlap is expected to be quite poor. This problem may be somewhat alleviated if one uses recently developed concentric-circle-grating surface-emitting semiconductor lasers,⁴ in which the light is coupled out through a circular surface grating. The modes of these sources are similar to those of Bragg fibers—both have a dark spot in the middle—and so the modal overlap would be expected to be good. Another way to improve coupling is the use of a Bragg fiber source. This can be achieved by suitably doping such a fiber, for example with erbium or neodymium, to give a source in the near-infrared part of the spectrum. These can be quite efficient by writing a standard photo-induced grating in the Bragg structure,¹² thus providing feedback in the propagation direction.

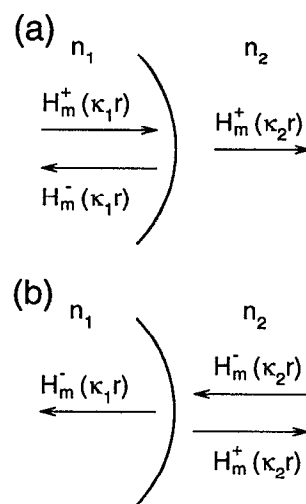


FIG. 10. (a) Reflection and transmission of an outgoing wave at a cylindrical interface. (b) Reflection and transmission of an incoming wave at a cylindrical interface.

We note that following earlier work on periodic¹³ and spherical¹⁴ systems, Bragg fibers also offer the potential for exhibiting a photonic band gap if the cylindrical structure is combined with a grating in the propagation direction. Used as a source, such structures would have advantages over conventional fiber sources such as low threshold and low noise.

In conclusion, we have studied the modes of Bragg fibers. Our calculations show that the presence of a mode requires that the structure should be sufficiently reflective (indicated by the moduli of the eigenvalues of the reflection matrix), and that a phase condition should be satisfied (indicated by the argument of these eigenvalues). We show that the losses of the TE mode can be made smaller than any of the other modes, and Bragg fibers could thus be used as modal filters—it can be guaranteed that the losses of all other modes are higher. Our estimate of the losses of Bragg fibers is based upon Eq. (10), which requires several approximations. In a more careful analysis the losses of the structure must be explicitly included by making β complex. In this case the somewhat unphysical requirement to have a source at infinity or at the origin can be dropped, while the losses simply follow immediately from the imaginary part of β . Such a more realistic calculation would also have to take explicit account of the dispersion of the constituents.

ACKNOWLEDGMENTS

The authors thank Dr. Simon Poole for many useful discussions and insights, particularly during the initial stages of this work. They thank Dr. Greg Forbes for electronic mail discussions. This work was supported by the Australian Research Council, and by the Australian Photonics CRC. The Optical Fiber Technology Centre is a member of the Australian Photonics CRC.

APPENDIX

In the first subsection of this Appendix we describe our method to determine the modes of the structure. In the remainder we state, without proof, some of the results used in the main text.

A. Mathematical method

To calculate the modes of Bragg fibers we use Chew's method⁹ with some minor modifications and a clearer notation. Here we briefly derive the main results. Consistent with Eq. (4), the symbols h_r , h_ϕ , and h_z are understood to mean the corresponding magnetic field components, multiplied by the vacuum impedance Z .

The azimuthal field components $e_\phi(r)$ and $h_\phi(r)$ are given in terms of the longitudinal field components $e_z(r)$, $h_z(r)$ by

$$\begin{bmatrix} e_\phi \\ h_\phi \end{bmatrix} = \Gamma_m \begin{bmatrix} e_z \\ h_z \end{bmatrix}, \quad (\text{A1})$$

where Γ_m is the linear operator

$$\Gamma_m = \begin{bmatrix} -m\beta/\kappa^2 r & (-ik/\kappa^2)d/dr \\ (ikn^2/\kappa^2)d/dr & -m\beta/\kappa^2 r \end{bmatrix}. \quad (\text{A2})$$

The longitudinal field components e_z and h_z for a given mode, characterized by $\omega = ck$, β and m , are expressible in any region with uniform refractive index n as a superposition of outgoing and ingoing Hankel functions $H_m^+(\kappa r)$ and $H_m^-(\kappa r)$. Where two media with differing refractive indices n_1 and n_2 meet, a solution of Maxwell's equations can be found in the form indicated schematically in Fig. 10(a). The field on the left may be written without prejudice in the form

$$\begin{bmatrix} e_z \\ h_z \end{bmatrix} = (H_m^+(\kappa_1 r) + H_m^-(\kappa_1 r)R_{m;12})\mathbf{a}_1, \quad (\text{A3})$$

where the 2×2 reflection matrix $R_{m;12}$ is as yet unspecified, and \mathbf{a}_1 is a two-rowed vector. Note that Eq. (A3) is completely general, as any linear combination of H_m^+ and H_m^- for e_z , and independently any linear combination H_m^+ and H_m^- for h_z can be written in this form. The field on the right of the interface may similarly be written as

$$\begin{bmatrix} e_z \\ h_z \end{bmatrix} = H_m^+(\kappa_2 r)T_{m;12}\mathbf{a}_1, \quad (\text{A4})$$

where the 2×2 transmission matrix $T_{m;12}$ is as yet unspecified.

The boundary conditions at the interface may now be used to determine the transmission and reflection matrices. Using Eqs. (A3) and (A4), the continuity of e_z and h_z requires that

$$(H_m^+(\kappa_1 r') + H_m^-(\kappa_1 r')R_{m;12})\mathbf{a}_1 = H_m^+(\kappa_2 r')T_{m;12}\mathbf{a}_1, \quad (\text{A5})$$

if r' is the interface coordinate. This equation must hold for any incident field amplitudes \mathbf{a}_1 and thus

$$H_{m;1}^+ + H_{m;1}^- R_{m;12} = H_{m;2}^+ T_{m;12}, \quad (\text{A6})$$

where we have used the abbreviated notation $H_{m;j}^+ = H_m^+(\kappa_j r')$, where $j=1,2$. The continuity of the azimuthal field components may be similarly obtained by using Eqs. (A1),

$$\Gamma_m^+(\kappa_1 r') + \Gamma_m^-(\kappa_1 r')R_{m;12} = \Gamma_m^+(\kappa_2 r')T_{m;12}, \quad (\text{A7})$$

where we have used the notation $\Gamma_{m;j}^\pm = \Gamma_{m;j} H_{m;j}^\pm$. As in Eq. (A5), all quantities in Eqs. (A6) and (A7) are evaluated at $r=r'$, the radius of the interface. Explicit expressions for the reflection and transmission matrices may now be obtained by elimination from Eqs. (A6) and (A7) giving the result

$$\begin{aligned} T_{m;12} &= (H_{m;1}^- \Gamma_{m;2}^+ - H_{m;2}^+ \Gamma_{m;1}^-)^{-1} \\ &\quad \times (H_{m;1}^- \Gamma_{m;1}^+ - H_{m;1}^+ \Gamma_{m;1}^-), \\ R_{m;12} &= (H_{m;1}^- \Gamma_{m;2}^+ - H_{m;2}^+ \Gamma_{m;1}^-)^{-1} \\ &\quad \times (H_{m;2}^+ \Gamma_{m;1}^+ - H_{m;1}^+ \Gamma_{m;2}^+). \end{aligned} \quad (\text{A8})$$

Generally similar expressions may be obtained for the matrices $T_{m;21}$ and $R_{m;21}$ for an incoming wave defined in Fig. 10(b). The result of such a calculation is

$$\begin{aligned} T_{m;21} &= (H_{m;1}^- \Gamma_{m;2}^+ - H_{m;2}^+ \Gamma_{m;1}^-)^{-1} \\ &\quad \times (H_{m;2}^- \Gamma_{m;2}^+ - H_{m;2}^+ \Gamma_{m;2}^-), \end{aligned}$$

$$R_{m;21} = (H_{m;1}^- \Gamma_{m;2}^+ - H_{m;2}^+ \Gamma_{m;1}^-)^{-1} \times (H_{m;2}^- \Gamma_{m;1}^- - H_{m;1}^+ \Gamma_{m;2}^-). \quad (\text{A9})$$

Note that all four reflection and transmission matrices in Eqs. (A8) and (A9) are diagonal for $m=0$.

A field in a many-layered structure may be obtained by superposition of the simple two-layer fields of Fig. 10. We may take layers 1 and 2 as a generic pair of adjacent layers, with additional layers at both sides. If layer 3 is the next layer on the right-hand side, the longitudinal fields in layer 1 may be written in the form

$$(H_{m;1}^+ + \tilde{R}_{m;12} H_{m;1}^-) \mathbf{a}_1, \quad (\text{A10})$$

and those in layer 2 as

$$(H_{m;2}^+ + \tilde{R}_{m;23} H_{m;2}^-) \mathbf{a}_2, \quad (\text{A11})$$

where $\tilde{R}_{m;12}$ and $\tilde{R}_{m;23}$ are again 2×2 matrices which are yet to be determined.

Consider the amplitude \mathbf{a}_2 of $H_m^+(\kappa_2 r)$ in layer 2. Referring to Fig. 10, this results from transmission of H^+ from layer 1, and from reflection of H^- from the interface between the layers. Thus,

$$\mathbf{a}_2 = T_{m;12} \mathbf{a}_1 + R_{m;21} \tilde{R}_{m;23} \mathbf{a}_2. \quad (\text{A12})$$

Similarly, the ingoing amplitude $\tilde{R}_{m;12} \mathbf{a}_1$ in layer 1 results from transmission of the ingoing amplitude $\tilde{R}_{m;23} \mathbf{a}_2$ in layer 2 and reflection of the outgoing amplitude \mathbf{a}_1 in layer 1, so that

$$\tilde{R}_{m;12} \mathbf{a}_1 = R_{m;12} \mathbf{a}_1 + T_{m;21} \tilde{R}_{m;23} \mathbf{a}_2. \quad (\text{A13})$$

Elimination of \mathbf{a}_1 and \mathbf{a}_2 from Eqs. (A12) and (A13) then gives the matrix equation

$$\tilde{R}_{m;12} = R_{m;12} + T_{m;21} \tilde{R}_{m;23} (1 - R_{m;21} \tilde{R}_{m;23})^{-1} T_{m;12}. \quad (\text{A14})$$

Equation (A14) and its analogues for other layers permit the successive determination of $\tilde{R}_{m;j,j+1}$ in all layers, given its value in one of the layers. Equation (A12) may then be used to determine successively the field amplitude vector \mathbf{a} in each layer, given its value in one of the layers. As mentioned above, the matrices T and R for $m=0$ are diagonal, and in consequence the matrices \tilde{R} are diagonal as well in this case. This means that the rotationally invariant $m=0$ modes separate into TE and TM.

Consider now a stack of $N+1$ layers in which layer 1 is the innermost layer, and layer $N+1$ is the infinite cladding layer. We formally seek a mode field purely outgoing in the cladding, implying that

$$\tilde{R}_{m;N,N+1} = R_{m;N,N+1}. \quad (\text{A15})$$

The right-hand side of this equation can be determined from the second of Eqs. (A8), while the others may be determined successively by Eq. (A14). The physical significance of $\tilde{R}_{m;12}$ is the matrix reflection from the entire stack when the incident field is an outgoing wave in the innermost layer. As pointed out in connection with Eqs. (5) and (6) the modal fields obtained in this way are singular at the origin, but they may nevertheless be interpreted as physically realizable, but imperfectly bound modes.

B. Conservation of power

The outgoing power P per unit area of cylindrical surface at radius r can be shown to be given by

$$P = \frac{1}{Z} \frac{k}{\pi \kappa^2 r} [n^2(|a^+|^2 - |a^-|^2) + |b^+|^2 - |b^-|^2], \quad (\text{A16})$$

where the column vector with the elements a^+, b^+ is the outgoing field amplitude vector \mathbf{a} , while that with elements a^-, b^- is the reflected field amplitude vector

$$\begin{bmatrix} a^- \\ b^- \end{bmatrix} = \tilde{R} \begin{bmatrix} a^+ \\ b^+ \end{bmatrix} = \tilde{R} \mathbf{a}. \quad (\text{A17})$$

Equation (A16) may be obtained from the expressions for the fields [Eq. (A3)] and Poynting's theorem, and making use of the Wronskian property of the Hänkel functions.¹⁵ We note that the product rP is necessarily the same in each layer.

C. Bound on the eigenvalues of $\tilde{R}_{m;12}$

Equation (A16) for the outgoing power can be used to show that the moduli of the eigenvalues of the innermost matrix $\tilde{R}_{m;12}$ cannot exceed unity. Let us denote this innermost matrix simply by \tilde{R} , and let \mathbf{a} be an eigenvector of \tilde{R} with eigenvalue λ (not necessarily close to unity), so

$$\tilde{R} \mathbf{a} = \lambda \mathbf{a}. \quad (\text{A18})$$

Since the outgoing power is positive by construction, it can then be shown that, using Eq. (A17) [cf. Eq. (A16)],

$$n^2 |a^-|^2 + |b^-|^2 < n^2 |a^+|^2 + |b^+|^2 \quad (\text{A19})$$

or

$$\begin{bmatrix} a \\ b \end{bmatrix}^\dagger \tilde{R}^\dagger \begin{bmatrix} n^2 & 0 \\ 0 & 1 \end{bmatrix} \tilde{R} \begin{bmatrix} a \\ b \end{bmatrix} < \begin{bmatrix} a \\ b \end{bmatrix}^\dagger \begin{bmatrix} n^2 & 0 \\ 0 & 1 \end{bmatrix} \begin{bmatrix} a \\ b \end{bmatrix}. \quad (\text{A20})$$

Substitution from Eq. (A18) then gives

$$|\lambda|^2 < 1. \quad (\text{A21})$$

D. Relationship between the intensity reflection coefficients of the stack and the eigenvalues of $\tilde{R}_{m;12}$

If $\begin{bmatrix} a^+ \\ b^+ \end{bmatrix}$ is an eigenvector of $\tilde{R}_{m;12} = \tilde{R}$, using the notation of Eqs. (A16) and (A17) we have

$$\lambda \begin{bmatrix} a^+ \\ b^+ \end{bmatrix} = \begin{bmatrix} a^- \\ b^- \end{bmatrix}. \quad (\text{A22})$$

The corresponding ratio of the reflected to the outgoing incident power P^-/P^+ [cf. Eq. (A16)] is accordingly given by

$$\frac{P^-}{P^+} = \frac{n^2 |a^-|^2 + |b^-|^2}{n^2 |a^+|^2 + |b^+|^2} = |\lambda|^2, \quad (\text{A23})$$

confirming the interpretation of $|\lambda|^2$ as a reflectivity.

¹ P. Yeh, A. Yariv, and E. Marom, J. Opt. Soc. Am. **68**, 1196 (1978).

² N. J. Doran and K. J. Blow, J. Lightwave Technol. **LT-1**, 588 (1983).

³ Strictly speaking this conclusion is valid only if the ambient refractive index is not too small. Otherwise, total internal reflection occurring on the fiber-ambient interface may lead to confinement similar to that in conventional fibers.

- ⁴T. Ergodan, O. King, G. W. Wicks, D. G. Hall, C. L. Dennis, and M. J. Rooks, *Appl. Phys. Lett.* **60**, 1773 (1992).
- ⁵H. A. MacLeod, *Thin-Film Optical Filters* (Hilger, Bristol, 1986).
- ⁶S. B. Poole, Optical Fiber Technology Centre, University of Sydney 2006, Australia (personal communication).
- ⁷A. W. Snyder and J. D. Love, *Optical Waveguide Theory* (Chapman and Hall, London, 1983).
- ⁸D. Marcuse, *Light Transmission Optics* (Van Nostrand, New York, 1982), Chap. 8.
- ⁹W. C. Chew, *Waves and Fields in Inhomogeneous Media* (Van Nostrand, New York, 1990), Chap. 3.
- ¹⁰M. Born and E. Wolf, *Principles of Optics*, 6th ed. (Pergamon, Oxford, 1980).
- ¹¹D. Marcuse, *Theory of Dielectric Optical Waveguides*, 2nd ed. (Academic, San Diego, 1991), Sect. 1.5.
- ¹²G. Meltz, W. W. Morey, and W. H. Glenn, *Opt. Lett.* **14**, 823 (1989).
- ¹³E. Yablonovitch and T. J. Gmitter, *Phys. Rev. Lett.* **67**, 2295 (1991).
- ¹⁴D. Brady, G. Papen, and J. E. Sipe, *J. Opt. Soc. Am. B* **10**, 644 (1993).
- ¹⁵M. Abramowitz and I.A. Stegun, *Handbook of Mathematical Functions* (Dover, New York, 1972), Ch. 9.